RARE METALS

ORIGINAL ARTICLE

Magnetic properties and anomalous Hall effect of Mn_3Sn thin films controlled by defects and ferroelectric $0.7Pb(Mg_{1/3}Nb_{2/3})O_3$–$0.3PbTiO_3$ substrate

Zhong-Ping Zhao* [ORCID], **Qi Guo, Feng-Hua Chen, Ke-Wei Zhang, Yong Jiang**

Abstract Noncollinear antiferromagnetic Mn_3Sn films have received much attention due to their potential applications in antiferromagnetic spintronic devices. In this work, single-phase polycrystalline antiferromagnetic Mn_3Sn thin films were successfully prepared by magnetron sputtering. The defects in the thin films were regulated by adjusting the sputtering power. The relationship among the films structure, the anomalous Hall effect (AHE) and the defects was investigated. High defect concentration in the Mn_3Sn films led to large room temperature ferromagnetic moments. The maximum saturation magnetization reached up to ~ 16 kA·m^{-1} (36 mμ_B/Mn), which was much larger than the values reported in literatures. The coercive field of 38 mT was obtained in a high-quality Mn_3Sn film, which effectively reduced the flipping magnetic field. Moreover, the anomalous Hall resistance and coercive field of the Mn_3Sn films prepared on the ferroelectric substrates were manipulated through an applied electric field, indicating that the piezoelectric stress has a great influence on the nonzero Berry curvature of the triangular spin structure in the antiferromagnetic materials. These results will promote the potential application of Mn_3Sn in high-density and low-power antiferromagnetic spintronic devices.

Keywords Noncollinear antiferromagnet; Mn_3Sn; Anomalous Hall effect; Ferromagnetic moment; Electric field manipulation

Z.-P. Zhao*, Q. Guo, F.-H. Chen, K.-W. Zhang, Y. Jiang
School of Materials Science and Engineering, Taiyuan University of Science and Technology, Taiyuan 030024, China
e-mail: zpzhao_sx@163.com

1 Introduction

The anomalous Hall effect (AHE) was observed in a bulk noncollinear antiferromagnetic Mn_3Sn by Nakatsuji et al. [1] in 2015, and its value was comparable to those of ferromagnetic materials. Subsequently, Mn_3Sn films became one of the hot spots in antiferromagnetic spintronics. Mn_3Sn is an antiferromagnetic material with a kagome lattice structure in the c-plane. Owing to the competition of exchange and Dzyaloshinskii–Moriya interactions, the 120° ordered Mn spins in the triangle are arranged in an inverse triangle structure and the magnetic moments cancel each other out [2–4]. In addition, a slight inclination in the triangular spin structure in c-plane results in a small net ferromagnetic spontaneous moment (~ 2 mμ_B/Mn) parallel to c-plane below the Néel point [5, 6]. Generally, AHE is related to the magnetic moment of ferromagnetic materials. Thus, the unconventional phenomenon in noncollinear antiferromagnetic materials has attracted great attention. It is generally believed that the origin of AHE in Mn_3Sn is related to nonzero Berry curvature [7–9]. Recent studies have shown that the AHE of antiferromagnetic Mn_3Sn originates from Weyl fermions caused by chiral antiferromagnetic spin structures. They behave like magnetic monopoles in momentum space and lead to a large Berry curvature, thus producing AHE [5, 10–12]. Antiferromagnetic Mn_3Sn also has the advantages of no magnetic field leakage and the ability to control the Hall resistance (R_{Hall}) by means of a small external magnetic field [1]. In addition, the latest research shows that the spin Hall effect and the inverse spin Hall effect can be achieved by manipulating the noncollinear spin in Mn_3Sn [13]. These features and the novel physical phenomena provide opportunities for the development and application of high-

performance spintronic devices, such as high-density magnetic random-access memories with low power consumption.

High quality of the Mn$_3$Sn film is the premise for its application in antiferromagnetic spintronic devices. Some groups have reported that polycrystalline Mn$_3$Sn [7, 14, 15] and single-crystalline Mn$_3$Sn [16, 17] films were grown by the magnetron sputtering method, which exhibited remarkable AHE. Ikeda et al. [15] found that manganese-rich Mn$_3$Sn films were necessary to reduce other impurity phases (such as Mn$_2$Sn phase) in the sample, thereby effectively enhancing the AHE. You et al. [16] studied the effect of an external magnetic field along different crystals on AHE in quasi-epitaxial Mn$_3$Sn films. However, the Hall resistivity in these studies was generally small, and the coercive field (H_c) in the anomalous Hall curve was greater than 0.3 T [7, 14–16], nearly ten orders of magnitude higher than that of a single-crystal bulk Mn$_3$Sn [1]. It is difficult to obtain low switching magnetic field of Mn$_3$Sn films, which creates difficulties for its future application in high-density spintronic devices. This phenomenon may be related to the inconsistent particle orientation or excessive defects in Mn$_3$Sn films.

Thus, obtaining high-quality Mn$_3$Sn films are crucial for controlling the H_c of AHE. However, there are only few reports on the defect regulation of Mn$_3$Sn films. On the other hand, electric field control of the magnetization and AHE is an extensively field due to its enormous potential application in spintronic devices with high speed, small size and low energy exhaust [18–20]. In strain-mediated magnetoelectric coupling mechanism, the (011)-oriented 0.7Pb(Mg$_{1/3}$Nb$_{2/3}$)O$_3$–0.3PbTiO$_3$ (PMN-PT) substrate has been widely selected for the anisotropy manipulation because of the large anisotropic piezoelectric coefficient [21–24]. In this work, Mn$_3$Sn films with different defect concentrations were prepared by the magnetron sputtering method, and the film growth rate was tuned by adjusting the sputtering power. A H_c of 38 mT in the anomalous Hall curve was obtained, and the Hall resistance and coercive field of Mn$_3$Sn films were regulated by the applied electric field.

2 Experimental

Mn$_3$Sn films with thickness of 40 nm were prepared on (111)-oriented MgO substrates by DC magnetron sputtering method using different sputtering powers. The sputtering target was Mn$_{3.1}$Sn alloy. In the experiment, the base pressure was 6.65×10^{-6} Pa. The Ar sputtering pressure was set to 0.665 Pa, and the substrate temperature was set to 200 °C. The sputtering powers of Mn$_{3.1}$Sn alloy targets were fixed at 30, 40, 50 and 70 W, and the corresponding

film growth rates were 0.016, 0.022, 0.032 and 0.043 nm·s^{-1}, respectively. The corresponding samples were marked as S-30, S-40, S-50 and S-70, respectively. The Mn$_3$Sn films grown on MgO substrates were annealed under vacuum at 500 °C to facilitate the crystallization of Mn$_3$Sn. In order to study the influence of the electric field on the properties of the Mn$_3$Sn film, the sample with a thickness of 60 nm was grown on the (011)-oriented PMN-PT substrate with the sputtering power fixed at 40 W.

The film structure was characterized by X-ray diffraction (XRD, Bruker D8 Advance) and transmission electron microscopy (TEM, FEI Tecnai G2 F20). The magnetic properties were measured by a superconducting quantum interference device (SQUID, Quantum Design MPMS-5). The magnetic field dependence of the transport was carried out using a conventional four-probe method. The Hall resistance was characterized by a physical properties measurement system (PPMS, Quantum Design PPMS-9) with the van der Pauw method. A linear ordinary Hall effect (OHE) contribution has been subtracted in the Hall resistance due to that the Hall resistance consists of OHE and AHE contributions in the Mn$_3$Sn films.

3 Results and discussion

Figure 1 shows XRD patterns of the Mn$_3$Sn films prepared by sputtering with sputtering powers of 30, 50 and 70 W, respectively. It can be seen from Fig. 1 that all the diffraction peaks of the films correspond to hexagonal D0$_{19}$ Mn$_3$Sn, indicating that the single-phase polycrystalline state was formed and dominated by the (002) orientation. As the sputtering power (growth rate) decreased, the crystallinity of the films and the intensity of diffraction peaks increased significantly. Generally, intermetallic alloys possess larger surface energies than the oxide substrate materials. This difference in surface energy results in
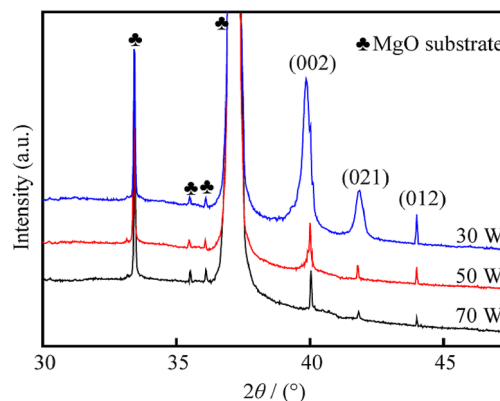

Fig. 1 XRD patterns of Mn$_3$Sn films deposited with different sputtering powers

the island-like growth of the films and more defects at the particle boundaries at high temperatures due to wetting problem [25]. In the case of low sputtering power of Mn_3Sn, small atomic flux density and low kinetic energy of metal atoms reaching the substrates resulted in a small deposition rate of Mn_3Sn. This facilitated the growth of flat atomic layers, thereby reducing the defects in the films and improving the crystal quality [26]. By comparing the position of the (002) diffraction peak of Mn_3Sn in Fig. 1 (shown by the dotted line), the (002) diffraction peak of the samples with low sputtering powers exhibited obvious blue shift, which further indicates few defects in the films.

To further illustrate the crystal structure of the Mn_3Sn films, Fig. 2 shows high-resolution TEM (HRTEM) and fast Fourier transform (FFT) images of the Mn_3Sn thin film prepared with the sputtering power fixed at 50 W (S-50 sample). It can be seen from Fig. 2a that there were some micro-regions with different lattice stripe spacings and orientations in the film. In combination with the FFT of thin film (Fig. 2b), it can be concluded that the S-50 sample has a polycrystalline structure. In order to determine the crystal structure of different micro-areas in the film, the reverse FFTs of the three micro-areas are shown in Fig. 2c–e, respectively. The interplanar spacings of 0.226, 0.208 and 0.217 nm correspond to the (002), (012) and (021) planes of the hexagonal crystal structure, respectively. These results are consistent with XRD data.

Next, the magnetic properties, magnetoresistance (MR) and AHE of the samples were evaluated. Figure 3 shows the magnetic hysteresis loops of the Mn_3Sn films with different sputtering powers measured at room temperature. The external magnetic field was applied parallel to the film plane. It can be seen that all samples displayed significant room temperature ferromagnetic characteristics, and the
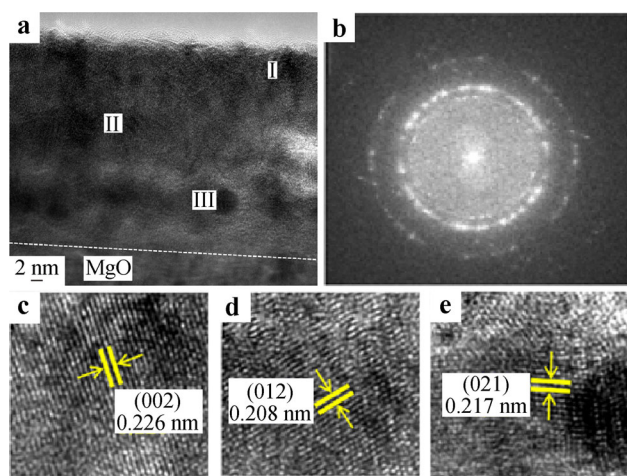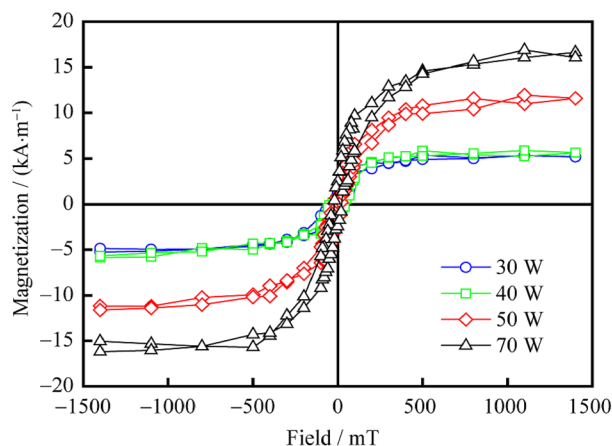

Fig. 3 Magnetic hysteresis loops of Mn_3Sn films deposited with different sputtering powers measured at room temperature

value of H_c was around 20 mT. The saturation magnetization (M_S) of samples prepared at sputtering powers of 30 and 40 W was about ~ 5 kA·m^{-1} (11 mμ_B/Mn). The M_S values of the samples using high sputtering power increased significantly, and the value of the S-70 sample reached ~ 16 kA·m^{-1} (36 mμ_B/Mn), which was much higher than the previously reported values [14, 15, 27]. This may be due to more defects in the film, leading to more uncompensated magnetic moments generated by the Mn atoms in the (001) plane and even the residual magnetic moments in the direction perpendicular to the (001) plane [16]. The increased concentration of defects was also reflected in the decreased diffraction peak intensity of the samples prepared using high sputtering powers in XRD patterns. In addition, theoretical and experimental studies have demonstrated that single-crystal Mn_3Sn hosts Weyl fermions [5, 28].

The magnetic field dependence of the MR curves for the Mn_3Sn thin film with the sputtering power fixed at 50 W
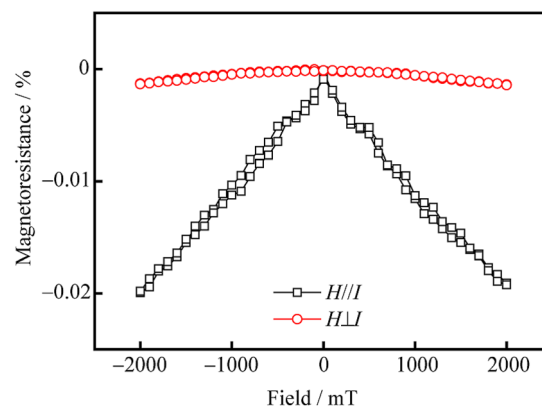

Fig. 2 **a** Cross-sectional HRTEM image and **b** FFT image of Mn_3Sn film with sputtering power fixed at 50 W; reverse FFT images of three nano-areas in **a**: **c** Area I, **d** Area II, and **e** Area III

Fig. 4 Magnetic field dependence of MR of Mn_3Sn film with sputtering power fixed at 50 W under a magnetic field parallel and perpendicular to current measured at room temperature

was carried out at room temperature using a conventional four-probe method, as shown in Fig. 4. Here, the magnetic field (H) was applied parallel and perpendicular to the current (I), and the maximum applied magnetic field was 2 T. The MR is defined as $MR = [R(H) - R(0)/R(0)] \times 100\%$, where $R(0)$ and $R(H)$ are the resistance at zero field and magnetic field (H). It can be seen that the value of negative MR is about 0.02% with the magnetic field parallel to the current, and the one is almost zero with the magnetic field perpendicular to the current, confirming the topological Weyl semimetal state realized in the single-phase polycrystalline Mn₃Sn films as reported in the Mn₃Sn single crystals [5, 28].

Figure 5 shows the room temperature anomalous Hall curves with significant hysteresis loop characteristics for the Mn₃Sn films prepared under different sputtering powers. Compared to the magnetic properties (Fig. 3), the value of H_c in the AHE is much higher than that of the magnetic hysteresis loops, which also indicates that ferromagnetism and AHE have different sources in the Mn₃Sn films. The magnetism comes from the canted Mn magnetic moment in the triangular spin structures [5, 6, 29], while AHE originates from nonzero Berry curvature of noncollinear antiferromagnetic materials [7–9]. From Fig. 6, it is evident that the H_c of the anomalous Hall curve decreased gradually with the decrease of sputtering power. The H_c value of the S-70 sample was found to be 290 mT, while that of S-30 sample reduced by an order of magnitude, to only 38 mT. This value was much smaller than that reported in Refs. [7, 14–16]. A small coercive field in the anomalous Hall loop can effectively reduce the reversal magnetic field, which is of great significance for high-density spintronic devices. It can be seen that the defect concentration in the films can be effectively tuned and the expected antiferromagnetic Mn₃Sn film with a small H_c can be obtained by regulating the sputtering power.
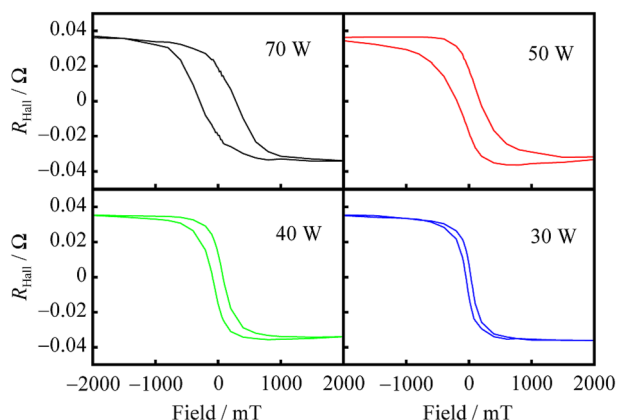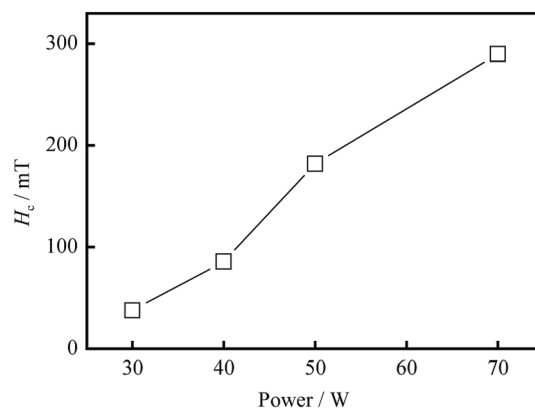

Fig. 6 Dependence of H_c of AHE on sputtering power in Mn₃Sn films

It is a good attempt for low-power piezoelectric strain manipulation in the application of antiferromagnetic Mn₃Sn films in magnetic storage devices with high-density and low-power. In order to study the effect of piezoelectric strain on the electrical transport properties of the films, a 60-nm-thick Mn₃Sn film deposited with the sputtering power fixed at 40 W was prepared on the (011)-oriented PMN-PT substrate. In order to clear the magnetic property of the Mn₃Sn film deposited on the PMN-PT substrate, the right inset in Fig. 7 shows the magnetic hysteresis loop of the Mn₃Sn film measured at room temperature, exhibiting room temperature ferromagnetic characteristics. Here, the magnetic field was applied parallel to the film plane. The M_S is $\sim$ 5.8 kA·m⁻¹ (12.8 mμ$_B$/Mn), which is slightly larger than that of the Mn₃Sn film deposited on the MgO substrate with the sputtering power fixed at 40 W. This may be due to more defects in the Mn₃Sn film on PMN-PT [16]. The AHE was carried out under different gate electric fields (E_G), and the external electric field was vertically applied to the film. The measurement schematic diagram is shown in the left inset in Fig. 7. It can be seen that when the E_G value was set to $-$ 2.3 and $-$ 4.2 kV·cm⁻¹, both the anomalous Hall resistance and the H_c of the Mn₃Sn film increased significantly, as shown in Fig. 7. When the external electric field was zero, the Hall resistance was 0.034 Ω, and the H_c was 85 mT. When E_G was set to $-$ 4.2 kV·cm⁻¹, the Hall resistance increased to 0.042 Ω and the H_c became 246 mT. It can be seen that the external electric field had a significant regulating effect on the AHE. As the length of Thomas–Fermi screening of metallic Mn₃Sn alloy is very short (less than 1 nm) [30], the electric field will be quickly screened at the film interface. Thus, it is impossible to affect the interior of Mn₃Sn film with a thickness of 60 nm. Therefore, the regulation of AHE by E_G should be realized by the piezoelectric strain of PMN-PT. Under the action of the electric field, the piezoelectric strain of PMN-PT substrate affects the Mn₃Sn film,
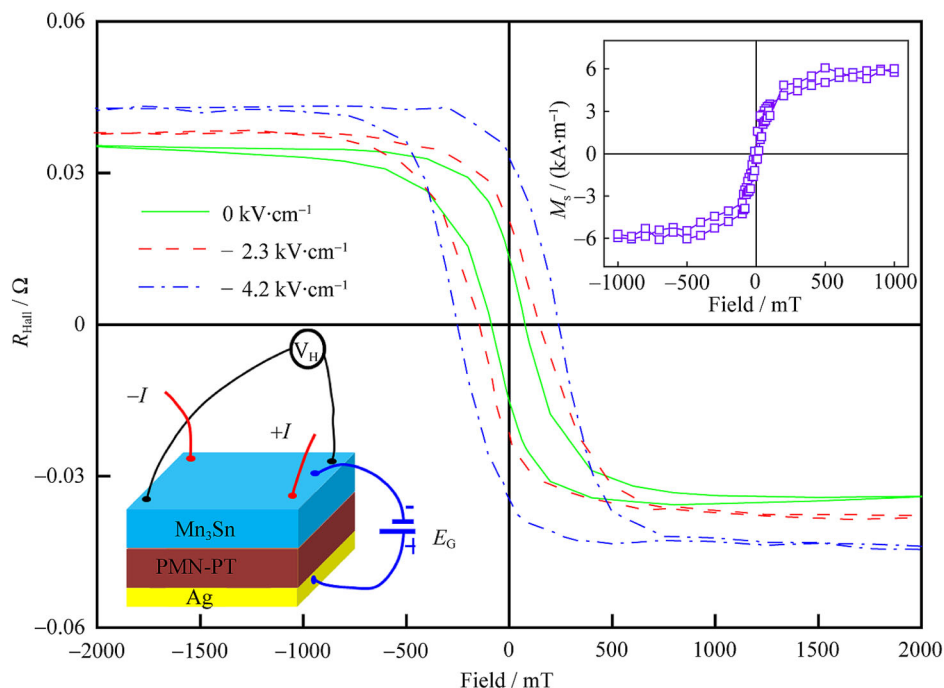

Fig. 5 Anomalous Hall curves of Mn₃Sn films deposited using different sputtering powers measured at room temperature

Fig. 7 Anomalous Hall curves of Mn_3Sn film deposited with sputtering power fixed at 40 W measured at room temperature under different gate electric fields; left inset being a schematic diagram of Hall resistance measurement with gate electric field perpendicularly applied across multilayered films; right inset showing hysteresis loop measured at room temperature

resulting in the deformation of the antiferromagnetic triangular spin structure. This gives rise to large Berry curvature and enhanced anomalous Hall resistance [31]. Moreover, there are more defects in Mn_3Sn films under strain, which results in a greater pinning effect of H_c.

4 Conclusion

In summary, noncollinear antiferromagnetic Mn_3Sn films were successfully prepared by the magnetron sputtering method, and the relationship among the magnetism, AHE and film defect concentration was studied. In the case of Mn_3Sn films, large defect concentration led to remarkable ferromagnetic moments at room temperature. The maximum value of M_S reached up to ~ 16 $kA \cdot m^{-1}$ (36 $m\mu_B$/Mn). By reducing the sputtering power and the film growth rate, high-quality Mn_3Sn films with effectively reduced defect concentration were obtained. The H_c of the films was controlled through the sputtering power and the minimum value of H_c reached 38 mT, facilitating the application for high-density and low-power antiferromagnetic spintronic devices. In addition, the anomalous Hall resistance and H_c of the Mn_3Sn film deposited on the piezoelectric PMN-PT substrate were tuned by the gate electric field, indicating that the piezoelectric strain at the interface has a significant effect on the nonzero Berry curvature of the triangular spin structure in the film.

References

[1] Nakatsuji S, Kiyohara N, Higo T. Large anomalous Hall effect in a non-collinear antiferromagnet at room temperature. Nature. 2015;527(7577):212.

[2] Qin PX, Yan H, Wang XN, Feng ZX, Guo HX, Zhou XR, Wu HJ, Zhang X, Leng ZGG, Chen HY, Liu ZQ. Noncollinear spintronics and electric-field control: a review. Rare Met. 2020; 39(2):95.

[3] Tomiyoshi S, Yamaguchi Y. Magnetic structure and weak ferromagnetism of Mn_3Sn studied by polarized neutron diffraction. J Phys Soc Jpn. 1982;51(8):2478.

[4] Brown PJ, Nunez V, Tasset F, Forsyth JB, Radhakrishna P. Determination of the magnetic structure of Mn_3Sn using generalized neutron polarization analysis. J Phys Condens Matter. 1990;2(47):9409.

[5] Kuroda K, Tomita T, Suzuki MT, Bareille C, Nugroho AA, Goswami P, Ochi M, Ikhlas M, Nakayama M, Akebi S, Noguchi R, Ishii R, Inami N, Ono K, Kumigashira H, Varykhalov A, Muro T, Koretsune T, Arita R, Shin S, Takeshi K, Nakatsujiet S. Evidence for magnetic Weyl fermions in a correlated metal. Nat Mater. 2017;16(11):1090.

[6] Ohmori H, Tomiyoshi S, Yamauchi H, Yamamoto H. Spin structure and weak ferromagnetism of Mn_3Sn. J Magn Magn Mater. 1987;70(1–3):249.

[7] Ikeda T, Tsunoda M, Oogane M, Oh S. Anomalous Hall effect in polycrystalline Mn_3Sn thin films. Appl Phys Lett. 2018;113(22): 222405.

[8] Xiao D, Chang MC, Niu Q. Berry phase effects on electronic properties. Rev Mod Phys. 2010;82(3):1959.

[9] Miyasato T, Abe N, Fujii T, Asamitsu A, Onoda S, Onose Y, Nagaosa N, Tokurae Y. Crossover behavior of the anomalous Hall effect and anomalous Nernst effect in itinerant ferromagnets. Phys Rev Lett. 2007;99(8):086602.

[10] Burkov AA, Balents L. Weyl semimetal in a topological insulator multilayer. Phys Rev Lett. 2011;107(12):127205.

[11] Wan X, Turner AM, Vishwanath A, Savrasov SY. Topological semimetal and Fermi-arc surface states in the electronic structure of pyrochlore iridates. Phys Rev B. 2011;83(20):205101.

[12] Kubler J, Felser C. Weyl fermions in antiferromagnetic Mn$_3$Sn and Mn$_3$Ge. Europhys Lett. 2017;120(4):47002.

[13] Kimata M, Chen H, Kondou K, Sugimoto S, Muduli PK. Magnetic and magnetic inverse spin Hall effects in a non-collinear antiferromagnet. Nature. 2019;565(7741):627.

[14] Higo T, Qu D, Li Y, Chien CL, Otani Y. Anomalous Hall effect in thin films of the Weyl antiferromagnet Mn$_3$Sn. Appl Phys Lett. 2018;113(20):202402.

[15] Ikeda T, Tsunoda M, Oogane M, Oh S. Improvement of large anomalous Hall effect in polycrystalline antiferromagnetic Mn$_{3+x}$Sn thin films. IEEE Tran Magn. 2019;55(7):1.

[16] You Y, Chen X, Zhou X, Gu Y, Zhang R, Pan F, Song C. Anomalous Hall effect-like behavior with in-plane magnetic field in noncollinear antiferromagnetic Mn$_3$Sn films. Adv Electron Mater. 2019;5(3):1800818.

[17] Markou A, Taylor JM, Kalache A, Werner P. Noncollinear antiferromagnetic Mn$_3$Sn films. Phys Rev Mater. 2018;2(5):051001.

[18] Lu X, Ju H, Liu S, Xi J, Li B. Perpendicular magnetic anisotropy and thermal stability in CoSiB/Pd multilayers. Chin J Rare Met. 2018;42(10):1054.

[19] Wang WG, Li M, Hageman S, Chien CL. Electric-field-assisted switching in magnetic tunnel junctions. Nat Mater. 2012;11(1):64.

[20] Cai K, Yang M, Ju H, Wang S, Ji Y, Li B, Edmonds KW, Sheng Y, Zhang B, Zhang N, Liu S, Zheng H, Wang K. Electric field control of deterministic current-induced magnetization switching in a hybrid ferromagnetic/ferroelectric structure. Nat Mater. 2017;16(7):712.

[21] Lai Z, Li C, Li Z, Liu X, Zhou Z, Mi W, Liu M. Electric field-tailored giant transformation of magnetic anisotropy and interfacial spin coupling in epitaxial γ'-Fe$_4$N/Pb(Mg$_{1/3}$Nb$_{2/3}$)$_{0.7}$Ti$_{0.3}$O$_3$(011) multiferroic heterostructures. J Mater Chem C. 2019;7(28):8537.

[22] Yang Y, Yao Y, Chen L, Huang H, Zhang B, Lin H, Luo Z, Gao C, Lu YL, Li X, Xiao G, Feng C, Zhao YG. Controlling the anomalous Hall effect by electric-field-induced piezo-strain in Fe$_{40}$Pt$_{60}$/(001)-Pb(Mg$_{1/3}$Nb$_{2/3}$)$_{0.67}$Ti$_{0.33}$O$_3$ multiferroic heterostructures. Appl Phys Lett. 2018;112(3):033506.

[23] Lai Z, Li P, Mi W. Magnetoelectric coupling in γ'-Fe$_4$N/Pb(Mg$_{1/3}$Nb$_{2/3}$)0$_7$Ti$_{0.3}$O$_3$ multiferroic heterostructures. J Appl Phys. 2019;126(11):113901.

[24] Liu M, Hao L, Jin T, Cao J, Bai J, Wu D, Wang Y, Wei F. Electric-field manipulation of coercivity in FePt/Pb(Mg$_{1/3}$Nb$_{2/3}$)O$_3$–PbTiO$_3$ heterostructures investigated by anomalous Hall effect measurement. Appl Phys Express. 2015;8(6):063006.

[25] Feng Z, Yan H, Liu Z. Electric-field control of magnetic order: from FeRh to topological antiferromagnetic spintronics. Adv Electron Mater. 2019;5(1):1800466.

[26] Lu RB, Ma ZH, Zhang TL, Jiang CB. Chemical synthesis of SmCo$_5$/Co magnetic nanocomposites. Rare Met. 2019;38(4):306.

[27] Wang X, Feng Z, Qin P, Yan H, Zhou X, Guo H, Leng Z, Chen W, Jia Q, Hu Z, Wu H, Zhang X, Jiang C, Liu Z. Integration of the noncollinear antiferromagnetic metal Mn$_3$Sn onto ferroelectric oxides for electric-field control. Acta Mater. 2019;181:537.

[28] Yang H, Sun Y, Zhang Y, Shi WJ, Parkin SSP, Yan B. Topological Weyl semimetals in the chiral antiferromagnetic materials Mn$_3$Ge and Mn$_3$Sn. New J Phys. 2017;19(1):015008.

[29] Duan TF, Ren WJ, Liu WL, Li SJ, Liu W, Zhang ZD. Magnetic anisotropy of single-crystalline Mn$_3$Sn in triangular and helix-phase states. Appl Phys Lett. 2015;107(8):082403.

[30] Abeles F, Lopez-Rios T, Tadjeddine A. Investigation of the metal-electrolyte interface using surface plasma waves with ellipsometric detection. Solid State Commun. 1975;16(7):843.

[31] Lukashev P, Sabirianov RF, Belashchenko K. Theory of the piezomagnetic effect in Mn-based antiperovskites. Phys Rev B. 2008;78(18):184414.